





Research article

Surface properties and hydrogen bonding of accelerator-free polyurethane dispersion/carboxylated nitrile butadiene rubber using crosslinker hybridisation

Ivy Gan^{1,2}, Wen Shyang Chow^{1*}, Siong Hui Khoo², Mohamad Danial Shafiq¹

¹School of Materials and Mineral Resources Engineering, Engineering Campus, Universiti Sains Malaysia, Nibong Tebal 14300, Penang, Malaysia.

²Le Inoova Sdn Bhd, Klang, Selangor, Malaysia

Received 7 March 2024; accepted in revised form 20 April 2024

Abstract. This study focuses on producing polyurethane dispersion (PUD)/carboxylated nitrile butadiene rubber (XNBR) blends with different types of crosslinkers without both accelerators and sulphur. Two types of crosslinkers: epoxide crosslinker and organo-modified siloxane, are introduced in the PUD/XNBR (blending ratio of 80:20). The zeta potential and particle size of the PUD/XNBR blends were determined using a dynamic light-scattering nanoparticle analyser. The chemical interaction and surface roughness of the PUD/XNBR blends were evaluated using Fourier transform infrared spectroscopy (FTIR) and atomic force microscopy (AFM). The zeta potential and particle size of the PUD were influenced by XNBR blending and the types of crosslinkers. FTIR observations indicate that the XNBR and the crosslinkers facilitated intermolecular hydrogen bonding and different extents of ordered hydrogen bonding. A higher degree of ordered hydrogen bonding can be associated with a higher surface roughness of the PUD/XNBR blends. Nevertheless, the hybrid crosslinkers can be used to achieve reasonable surface roughness for the easier donning of latex gloves. The research findings can be applied to design glove products with desirable surface roughness and intermolecular bonding.

Keywords: elastomers; polyurethane, crosslinking agent, synthetic rubber, mixing, hydrogen bonding

1. Introduction

Polyurethane dispersions (PUD) have an extensive range of applications across a broad spectrum of industries, which include marine, automobile, and industry maintenance [1–5]. The urgent need for sustainable and environmentally friendly development in the research field [6] has further reiterated the significance of integrating PUD [7, 8]. The low-level emissions of volatile organic compounds [9] and their tailorable properties have contributed substantially to a wide array of applications [10, 11]. PUD applications can be found in adhesives, sealants, low-gloss coatings, decorative coatings, and protective coatings for wood, fibres, textiles, and metal [12–16].

Despite the environmental benefits of PUD, some of its limitations are worth mentioning. For example, the linear molecular structure of PUD often causes lower heat resistance and barrier properties compared to conventional solvent-based PUD [17–19]. PUD consisting of ester groups could make it vulnerable to hydrolysis and esterase degradation, further diminishing its properties [11, 20]. Additionally, the poor water resistance of PUD leads to a protracted drying process that necessitates an extended period [21, 22]. The blending of polyurethane dispersion (PUD) has primarily been applied in coating applications, with limited exploration in the context of dipped goods. Blending PUD with other polymers has emerged as

*Corresponding author, e-mail: shyang@usm.my

© BME-PT

a potential solution to address the limitations of PUD. Carboxylated nitrile butadiene rubber (XNBR) stands out as a highly favourable choice for blending with PUD due to its remarkable attributes, including superior abrasion resistance as well as solvent- and oil resistance [23, 24]. Additionally, recent research has highlighted the potential of carboxylated groups to facilitate ionic bonding, which can be combined with covalent sulphur bonding to reduce the required sulphur dosage [25–27]. Various approaches have been explored to blend polyurethane (PU) with nitrile butadiene rubber (NBR) to combine their advantageous properties. Düşünceli *et al.* [28], Tahir *et al.* [23], and Yan *et al.* [24] successfully produced a PU blend with enhanced performance by using crosslinkers, which still required conventional sulphur vulcanisation. In pursuing sulphur-free blends, researchers realised the hydrogen interaction between PU and XNBR and seized this opportunity to explore alternatives to sulphur crosslinking in the vulcanisation system. However, they still encountered challenges during the blending process of these two polymers because they had poor compatibility and inferior mechanical properties compared to pure PU [29, 30]. This highlighted that continual exploration of novel crosslinkers and evaluation of their feasibility with various PUD/XNBR blending systems are crucial areas for development within this field.

Various crosslinkers have been employed in individual XNBR and PUD systems, demonstrating the potential for improvement in these systems. In the case of XNBR, the traditional sulphur-based crosslinker has been widely used for vulcanisation. Another alternative approach to crosslinking XNBR involves using epoxidised soybean oil as a crosslinker [31]. However, it is worth noting that in this approach, fillers such as carbon black are still employed in the system to achieve satisfactory mechanical properties. Resol resins, in combination with silanes, have also been explored as crosslinkers for XNBR [32]. Trimethylolpropane tris(3-mercaptopropionate), when exposed to UV irradiation, has demonstrated its feasibility as a crosslinker for XNBR [33]. However, it is essential to note that crosslinkers in XNBR may necessitate UV irradiation or combination with other crosslinkers as an essential component of the crosslinking process. Additionally, magnesium aluminium layered double hydroxide and polyhedral oligomeric silsesquioxane have shown promising results, achieving maximum tensile strengths of 23.8 MPa [34, 35]

and 7.17 MPa [36] respectively, in crosslinked XNBR compounds.

In the present study, epoxide crosslinkers and organo-modified siloxane are utilised as crosslinkers, as these two crosslinkers do not have any nitrosatable properties and do not contain any functional groups that will provoke type IV allergies. By utilising hydrogen bonding as the main interaction between PUD and XNBR, together with the crosslinkers, it becomes possible to address the shortcomings of PUD while eliminating the need for sulphur and accelerators in the vulcanisation process of XNBR. Therefore, the objective of the present study is to develop PUD/XNBR blends (PUD: XNBR blending ratio of 80:20) to use crosslinkers as alternatives to sulphur and accelerators, particularly in dipped product applications without compromising the chemical and mechanical properties of the polymer. This blending approach creates a win-win situation by enhancing the overall properties and sustainability of the resulting polymer material. Additionally, the novelty of this study is that it focuses on unravelling the relationship between the degree of order hydrogen bonding and surface roughness. This study explores the extent of hydrogen bonding induced by different crosslinkers. The degree of ordered hydrogen bonding plays a pivotal role in shaping the surface roughness of the produced polymer blends, eventually affecting the surface texture properties. Hence, the relationship between the degree of ordered hydrogen bonding and the surface quality of the PUD/XNBR blends is unveiled at the end of this study.

2. Material and methods

2.1. Materials

Polyester polyurethane dispersion (Baymedix CD105) was supplied from Covestro AG (Germany) at a total solid content of 50%. KNL 830 grade of carboxylated nitrile butadiene rubber (XNBR) was obtained from Korea Kumho Petrochemical Co., Ltd. (Korea) with a total solid content (TSC) range of 44–46%. Calcium nitrate at a concentration of 54–56% and solid flakes of potassium hydroxide (KOH) were purchased from May Chern Chemicals Sdn Bhd. (Malaysia). Zinc oxide (ZnO) at a TSC of 50% was acquired from Farben Technique (M) Sdn. Bhd. (Malaysia). The epoxide crosslinker with grade Actival X351 and the organo-modified siloxane crosslinker with grade Actival K331 were supplied by Inoova Material Science Sdn. Bhd. (Malaysia).

2.2. Sample preparation

A coagulant compound containing (12%) calcium nitrate was prepared and allowed to mix for 24 h before the dipping process. A total of five compounds were prepared, as outlined in (Table 1). The compounded PUD and different PUD₈₀/XNBR₂₀ blend compositions were stirred using a mechanical stirrer (IKA RW 20, Germany) for 24 h. The formers were cleaned and dried in an oven (Memmert UF110, Germany) before being subjected to the dipping process. The formers were maintained at a temperature of 70 °C and immersed in a coagulant bath with the temperature control set at 50 °C by using a hot plate magnetic stirrer (Vevor 85-2, China). Afterwards, the coagulant-coated formers were dried in an oven for 3 min before being dipped into the desired compounded formulation. The former temperature was maintained at 60 °C before the dipping process. Subsequently, the latex-coated formers were subjected to gelation at 100 °C for 1 min, followed by a pre-leaching process at 50 °C for 1 min.

The resulting film was cured at temperatures of 60–65 °C (time = 10 min), followed by 65–70 °C (time = 10 min). Afterwards, the film underwent a post-leaching at 50 °C before being dried in an oven (Memmert UF110, Germany) at 100 °C for 5 min. Finally, the dried film was allowed to cool to room temperature before undergoing the stripping process.

2.3. Sample characterisation

2.3.1. Zeta potential

The particle size and zeta potential analysis for the compounded formulations was conducted using a dynamic light scattering (DLS) nanoparticle analyser (SZ-100V2, Horiba, Japan) at a temperature of 25 °C. Before the measurements, the samples were diluted by a factor of 100, and the obtained data represents the average reading from three separate measurements.

2.3.2. Fourier transform infrared spectroscopy (FTIR)

The FTIR spectra of the compounded formulations were analysed using attenuated total reflectance Fourier transform infrared spectroscopy (Nicolet iS5, Thermo Fisher, USA). The prepared blends were scanned 16 times in the wavelength range of 4000 to 500 cm⁻¹, with a resolution of 4 cm⁻¹. The degree of hydrogen bonding for each of the samples is acquired through Equation (1) [37]:

$$\begin{aligned} \text{Degree of hydrogen bonding} &= \\ &= \frac{A_{\text{hb}(1643-1661)} + A_{\text{hb}(1685-1689)} + A_{\text{hb}(1708-1711)}}{A_{\text{hb}} + A_{\text{nhb}(1728-1731)}} \end{aligned} \quad (1)$$

where A_{hb} is the area of hydrogen bonded fraction, A_{nhb} is the area of non-hydrogen bonded fraction, the corresponding area can be obtained by performing curve fitting based on a Gaussian distribution. By having the same procedure, the degree of ordered hydrogen bonding can be determined through Equation (2) [37]:

$$\begin{aligned} \text{Degree of ordered hydrogen bonding} &= \\ &= \frac{A_{\text{hb}(1643-1661)} + A_{\text{hb}(1685-1689)}}{A_{\text{hb}} + A_{\text{nhb}(1728-1731)}} \end{aligned} \quad (2)$$

2.3.3. Atomic force microscopy (AFM)

The topology and image of the samples were examined using an AFM (NX-10, Park System, Korea) under ambient conditions. The samples were prepared using a non-contact technique with dimensions of 2×2 cm with a scan range of 20×20 μm. The obtained image was then analysed using XEI (Park Systems Corporation) software.

3. Results and discussion

3.1. Particle size and zeta potential

The stability and particle size of the samples have been examined and tabulated in Table 2. The zeta

Table 1. Materials compositions and designation of the PUD₈₀/XNBR₂₀ blends with and without crosslinkers.

Ingredients [phr]	PUD ₈₀ /XNBR ₂₀ blends				
	PUD	PUD ₈₀ /XNBR ₂₀	PUD ₈₀ /XNBR ₂₀ /E ₁	PUD ₈₀ /XNBR ₂₀ /S ₁	PUD ₈₀ /XNBR ₂₀ /E _{0.5} S _{0.5}
PUD	100	80	80	80	80
XNBR	0	20	20	20	20
KOH	1.8	1.8	1.8	1.8	1.8
ZnO	1.0	1.0	1.0	1.0	1.0
Actival X351	0	0	1.0	0	0.5
Actival K331	0	0	0	1.0	0.5

Notes: E₁: Actival X351; S₁: Actival K331

Table 2. Zeta potential and particle size for pristine PUD, PUD₈₀/XNBR₂₀ blend, and PUD₈₀/XNBR₂₀ blend with different crosslinkers.

Materials designation	Zeta potential [mV]	Particle size [nm]
PUD ₁₀₀	−63.5 (SD:0.6)	209.9 (SD: 0.5)
PUD ₈₀ /XNBR ₂₀	−67.0 (SD:0.1)	174.7 (SD: 0.1)
PUD ₈₀ /XNBR ₂₀ /E ₁	−72.2 (SD:0.4)	171.2 (SD: 1.3)
PUD ₈₀ /XNBR ₂₀ /S ₁	−65.2 (SD:0.7)	189.9 (SD: 0.2)
PUD ₈₀ /XNBR ₂₀ /E _{0.5} S _{0.5}	−70.2 (SD:1.1)	193.8 (SD: 0.6)

potential for all samples showed negative charges, suggesting that the surfaces of the formulations are negatively charged or can be related to the anionic behaviour of the PUD [38]. Moreover, the zeta potential of the pristine PUD showed that it is less negatively charged among all the samples, which may be attributed to the blending of XNBR into PUD for the rest of the samples. The carboxylic group originating from the XNBR will be the main contributor to the increment of zeta potential towards a more negative value as the presence of the COO[−] had further increased the thickness of the electrical double layer of the PUD particle, encouraging stability by increasing repulsion between the PUD particles [39, 40].

By comparing the impact of the crosslinker on the zeta potential, the epoxide crosslinker in sample PUD₈₀/XNBR₂₀/E₁ will have a higher zeta potential compared to the organo-modified siloxane crosslinker in sample PUD₈₀/XNBR₂₀/S₁. This may be attributed to the chain structure of the crosslinker. Given that the structure of the organo-modified siloxane crosslinker is a copolymer that consists of ethylene oxide (EO) and propylene oxide (PO), the repeating unit of the PO may be higher than EO, and this imparts hydrophobicity to the sample PUD₈₀/XNBR₂₀/S₁. This phenomenon is similar to the study conducted by Sis and Birinci [41], in which they performed zeta potential studies on different types of surfactants with varying ratios of EO and PO. They also discovered that surfactants with higher concentrations of propylene oxide would reduce the zeta potential owing to their hydrophobicity. The hydrophobic behaviour of the organo-modified siloxane crosslinker caused lesser polar charges to appear on the particle's surface and eventually lowered the magnitude of the zeta potential [42]. As a result, lesser surface charges offer higher electrostatic repulsion and reduce the stability of the particles. Therefore, the sample of PUD₈₀/XNBR₂₀/E_{0.5}S_{0.5} consists of both crosslinkers of epoxide and organo-modified siloxane and

resembles the surface charges imparted by each crosslinker, resulting in a zeta potential value that lies between the zeta potential values of samples PUD₈₀/XNBR₂₀/E₁ and PUD₈₀/XNBR₂₀/S₁.

The formulation's particle size depends on the concentration of the ions on the surface of the particle. Particles with a higher ionic concentration tend to have a smaller size, as the respective particle will need to increase its surface area to accommodate additional ionic species [20]. This also explains why the blended or crosslinked formulations are smaller than the pristine PUD, as more polymers and additives are added to the compound. PUD₈₀/XNBR₂₀ contains XNBR molecules with a carboxylate group (COO[−]) that increases the ionic concentration of the particles [43]. The PUD₈₀/XNBR₂₀/S₁ has a higher particle size due to its hydrophobicity among the three crosslinked formulations. Epoxide crosslinker, which is more hydrophilic than organo-modified siloxane, contains more polar groups that can confer more ionic charges, increasing the surface area of the particles. The sample PUD₈₀/XNBR₂₀/E_{0.5}S_{0.5} exhibits the largest particle sizes among all the samples, possibly attributed to the interaction of the two types of crosslinkers, which might have countered the charges and consequently resulted in an increase in particle size.

3.2. FTIR analysis

Figure 1 shows the FTIR spectra of pristine PUD, PUD₈₀/XNBR₂₀ blend, and PUD₈₀/XNBR₂₀ blends with different types of crosslinkers. The spectra 3348–3392 cm^{−1} had been shown in all samples, and these peaks were responsible for the assignment of N–H stretching in the PUD. Moreover, the pristine PUD showed the stretching band of N–H stretching at 3348 cm^{−1}, while PUD₈₀/XNBR₂₀ showed some N–H stretching shifting to 3365 cm^{−1} and the crosslinked PUD blends showed further shifting in the range 3382–3392 cm^{−1}. This indicated that the incorporation of XNBR and crosslinkers caused N–H stretching disruption from the pristine PU and resulted in a shift of the wavenumber for N–H stretching. The shifting of the N–H stretching in the sample PUD₈₀/XNBR₂₀/E₁ may be contributed by the epoxide crosslinker's interaction with the PUD₈₀/XNBR₂₀. This finding was similar to Nuraini *et al.* [44], whereby they modified PU/silica with an epoxide group and detected the spectra of the N–H group of PU in the modified PU composite, which appeared

at around 3397 cm^{-1} . These spectra could be attributed to the hydroxyl group of the epoxide-modified PU and had overlapped with the spectra of N–H of PU, which led to the shifting of the peak to a higher wavenumber. Furthermore, there was a similar contribution from the crosslinker in PUD₈₀/XNBR₂₀/S₁ and this observation was similar to the work done by Phung *et al.* [45] and Apekis *et al.* [46]. Phung *et al.* [45] had crosslinked PUD with a copolymer of ethylene oxide-propylene oxide while Apekis *et al.* [46] used different ratios of soft segment and hard segment prepolymers to crosslink PU polymer; both noticed the shifting of the N–H stretching band. According to Apekis *et al.* [46], the shifting of N–H stretching to a higher wavenumber was due to the reduction of the N–H stretching of the urethane bond owing to the interruption of other chemical crosslinking in the PU.

Besides that, the characteristic peak of PUD was found in all the samples. C–H stretching of PUD had appeared in all samples within $2921\text{--}2935\text{ cm}^{-1}$ [47]. The presence of the peak within the range $2850\text{--}2863\text{ cm}^{-1}$ in all samples is attributed to the stretching of C–H methyl from PUD [48]. In addition, none of the samples showed the presence of the peak at 2270 cm^{-1} denoting that pristine PUD, PUD₈₀/XNBR₂₀ blends, and crosslinked PUD/XNBR blends are free from any isocyanate monomers [42, 49]. All of the samples showed spectra of $1728\text{--}1729\text{ cm}^{-1}$, indicating that polyester groups existed in all samples despite crosslinking systems being incorporated into the PUD/XNBR blending compounds [47, 50]. Furthermore, the typical peak of PUD had also been evinced in the range of $1632\text{--}1650$, $1562\text{--}1573$, $1530\text{--}1540$ and 1076 cm^{-1} . These peaks correspond to the C=C of the urethane group, C–N–H stretching, C–N stretching of that connected with the N–H group, and C–O of the urethane group, respectively [42, 51, 52]. Apart from that, the presence of XNBR in all of the blended compounds produced is evidenced by the spectra at $2236\text{--}2237$ and 969 cm^{-1} . These two peaks are responsible for the stretching vibration of C≡N from the acrylonitrile and the stretching of the trans-bond of C=C for the backbone of XNBR, respectively [53, 54].

With the exclusion of the samples of pristine PUD and PUD₈₀/XNBR₂₀, there are only crosslinked PUD₈₀/XNBR₂₀ blends, PUD₈₀/XNBR₂₀/E₁, PUD₈₀/XNBR₂₀/S₁ and PUD₈₀/XNBR₂₀/E_{0.5}S_{0.5}, which have the transmittance peak within $1453\text{--}1454$ and

$1434\text{--}1435\text{ cm}^{-1}$. These three samples have a common functional group in their crosslinkers, whereby all main backbones of the crosslinkers are made up of siloxane functional groups. Therefore, the presence of these peaks might correspond to the bending vibration of Si(CH₂). This finding is similar to Kapgate *et al.* [55] and Zhang *et al.* [56], who produced silane-treated nitrile rubber and epoxide composites that consist of silane treated silica and silane functionalized silicone nitride, respectively. Both of their studies observed spectra at 1450 and 1454 cm^{-1} in their FTIR characterisation. Besides, the peak $1434\text{--}1435\text{ cm}^{-1}$ could be attributed to the vibration of the CH₂ stretching that had been detected in siloxane-based polyurethane in the studies conducted by Zia *et al.* [57] Thus, the existence of these two peaks well denotes the presence of siloxane crosslinkers in the crosslinked blending compounds.

On top of that, the characteristic peaks of the siloxane groups Si–O–C, C–Si and Si–CH₂ which usually appeared at around $1245\text{--}1290\text{ cm}^{-1}$ had been observed in all samples. For instance, Su *et al.* [58] produced a block copolymer of polyurethane-polysiloxane, and the peak assignment of Si–O–C was found at 1251 cm^{-1} . Sousa *et al.* [59] synthesised organic-inorganic material by imidazole derivatives and observed symmetric bending of C–Si bonding within the $1245\text{--}1261\text{ cm}^{-1}$ range. However, all the samples were found to have peaks at $1252\text{--}1253\text{ cm}^{-1}$ regardless of the absence of siloxane crosslinker in pristine PUD and PUD₈₀/XNBR₂₀. These indicate that the characteristic peaks of the siloxane group may tend to overlap with the unsymmetric stretching of (C–O–C) at about $1138\text{--}1250\text{ cm}^{-1}$ that originated from the ester group of the PUD, as evidenced by a few studies [60–62]. Ma *et al.* [63] modified epoxy resin using silicone compounds and observed the bending of Si–CH₂ at around $1250\text{--}1290\text{ cm}^{-1}$. In their study, two different types of silicone compounds were utilised: glycidoxypopyl trimethoxysilane (GPTMS) and anilinomethyl triethoxysilane. They also observed the overlapping of the bending of Si–CH₂ at the range of $1250\text{--}1290\text{ cm}^{-1}$. Moreover, Byczyński [64] synthesised a polyurethane-siloxane that had been modified with different siloxane side chains and also noticed that the characteristic band of siloxane could not be identified due to the overlapping of the amide band at around 1230 cm^{-1} . They also deduced that only significant loading of the siloxane compound in the formulation

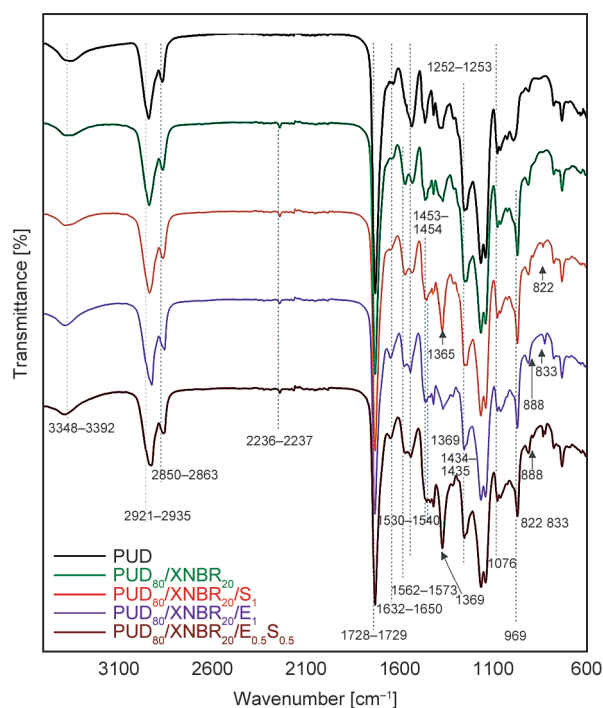


Figure 1. FTIR spectra of pristine PUD, PUD₈₀/XNBR₂₀ blend, and PUD₈₀/XNBR₂₀ blends with different types of crosslinkers.

was able to show the presence of the spectra for the siloxane group. Therefore, in this present study, all the samples, regardless of the introduction of the crosslinker, have a peak within 1252–1253 cm⁻¹ due to the small loading of the siloxane crosslinker and the overlapping of the ester group from PUD.

In addition, the existence of the organo-modified siloxane crosslinker can be observed through the distinctiveness shown by sample PUD₈₀/XNBR₂₀/S₁, whereby only this sample has a peak at around 1365 and 822 cm⁻¹. This respective spectra of 1365 cm⁻¹ could be attributed to the CH₃ bending of the block copolymer of EO and PO attached to the backbone of the organo-modified siloxane crosslinker [65]. Furthermore, Dai *et al.* [66] synthesised polydimethylsiloxane (PDMS) with copolymers of EO and PO and had a transmittance peak for the rocking of Si–CH₃ at around 802 cm⁻¹. Nonetheless, in this study, the introduction of an organo-modified siloxane crosslinker into PUD₈₀/XNBR₂₀/S₁ showed a vibration peak at 822 cm⁻¹. The shifting of the peak of Si–CH₃ may be owing to the fact that the backbone of the siloxane crosslinker is made up of polyether-siloxane with different monomer units of a copolymer of EO and PO, which therefore causes a different stretching wavenumber compared with PDMS copolymerise with EO and PO. Thus, the FTIR peak

at 822 cm⁻¹ could be mainly due to the vibration stretching of Si–CH₃ from the copolymer of organo-modified siloxane after being introduced into the PUD₈₀/XNBR₂₀ blending system.

The sample PUD₈₀/XNBR₂₀/E₁ showed a sharp peak at about 1369 cm⁻¹, unlike the sample PUD₈₀/XNBR₂₀/S₁, which had a peak at 1365 cm⁻¹. This peak may be attributed to the stretching of the epoxy ring, which is usually at 1340–1342 cm⁻¹. This peak was found to shift to a higher wavenumber after being incorporated into PUD₈₀/XNBR₂₀/E₁. Moreover, the characteristic peak for the stretching vibration peak of the epoxide crosslinker that is incorporated in PUD₈₀/XNBR₂₀/E_{0.5}S_{0.5} can be observed at 833 cm⁻¹, and this finding was very close to the peak observed by Zeng *et al.* [67] who had produced a coating of bis-silane epoxide from GPTMS and was found to have a peak at around 829 cm⁻¹. Nuraini *et al.* [44] modified PU with an epoxide group and also obtained a peak at 833 cm⁻¹. These findings could indicate that the incorporation of an epoxide crosslinker into PUD₈₀/XNBR₂₀/E₁ results in the assignment of Si–CH₃ at 833 cm⁻¹. In addition, the peak of 888 cm⁻¹ was also found to appear in the sample of PUD₈₀/XNBR₂₀/E₁. The presence of these peaks in PUD₈₀/XNBR₂₀/E₁ may be due to the stretching of the oxirane ring, which is usually found in the range of 851–915 cm⁻¹ [44, 68]. After all, the sample PUD₈₀/XNBR₂₀/E_{0.5}S_{0.5}, which contained both crosslinkers, resembled all the characteristic peaks from organo-modified siloxane at about 1371, 822 cm⁻¹ and typical peaks from epoxide crosslinkers at 1369, 833 and 888 cm⁻¹ finding suggested that both crosslinkers had been successfully introduced into the PUD₈₀/XNBR₂₀/E_{0.5}S_{0.5} blending compounds.

Figure 2 shows the deconvoluted peak for pristine PUD, PUD₈₀/XNBR₂₀ blend, and PUD₈₀/XNBR₂₀ blends with different types of crosslinkers. The hydrogen bonding in PUD is an important indicator of understanding the chemical interaction, particularly the involvement of XNBR and crosslinkers that connect with the backbone of the PUD. The ordered hydrogen bonding in PU is intricately linked to its structure-property relationships, primarily governed by the composition of soft and hard segments within its backbone. In our study, PUD is utilised, where the soft segment comprises polyester and the hard segment consists of urethane groups. The key to facilitating hydrogen bonding lies in fulfilling two main criteria: the presence of a proton donor and a

proton acceptor [69, 70]. Within the PUD structure, the N–H groups from the urethane units serve as proton donors, while the carbonyl groups (C=O) from the ester group act as proton acceptors. Notably, the N–H groups in the hard segment exhibit self-association, whereas the C=O groups in the soft segment lack such properties. The introduction of XNBR chains, which contribute additional C=O groups as acceptor units, causes a competitive scenario against self-association. This competition fosters a new form of interaction known as inter-association, where N–H groups from the urethane hard segment form hydrogen bonds with C=O bonds from the XNBR. This interaction disrupts the phase of the PUD, impacting its ability to form ordered hydrogen bonding or phase separation domains. Consequently, the

introduction of XNBR creates more opportunities for hydrogen bonding interactions, potentially leading to regions within the samples exhibiting some degree of order. The manifestation of these hydrogen bonding interactions can be observed through the shifting of wavenumbers in FTIR spectra, analysed via deconvolution of the carbonyl group using a Gaussian function [29, 70]. In essence, the theory behind ordered hydrogen bonding elucidates how the interaction between N–H and C=O groups, facilitated by the introduction of XNBR, alters the phase behaviour of PUD, ultimately influencing its material properties and performance. Therefore, the deconvolution of the carbonyl group by a Gaussian function will be the point of interest in understanding the distribution of hydrogen bonding,

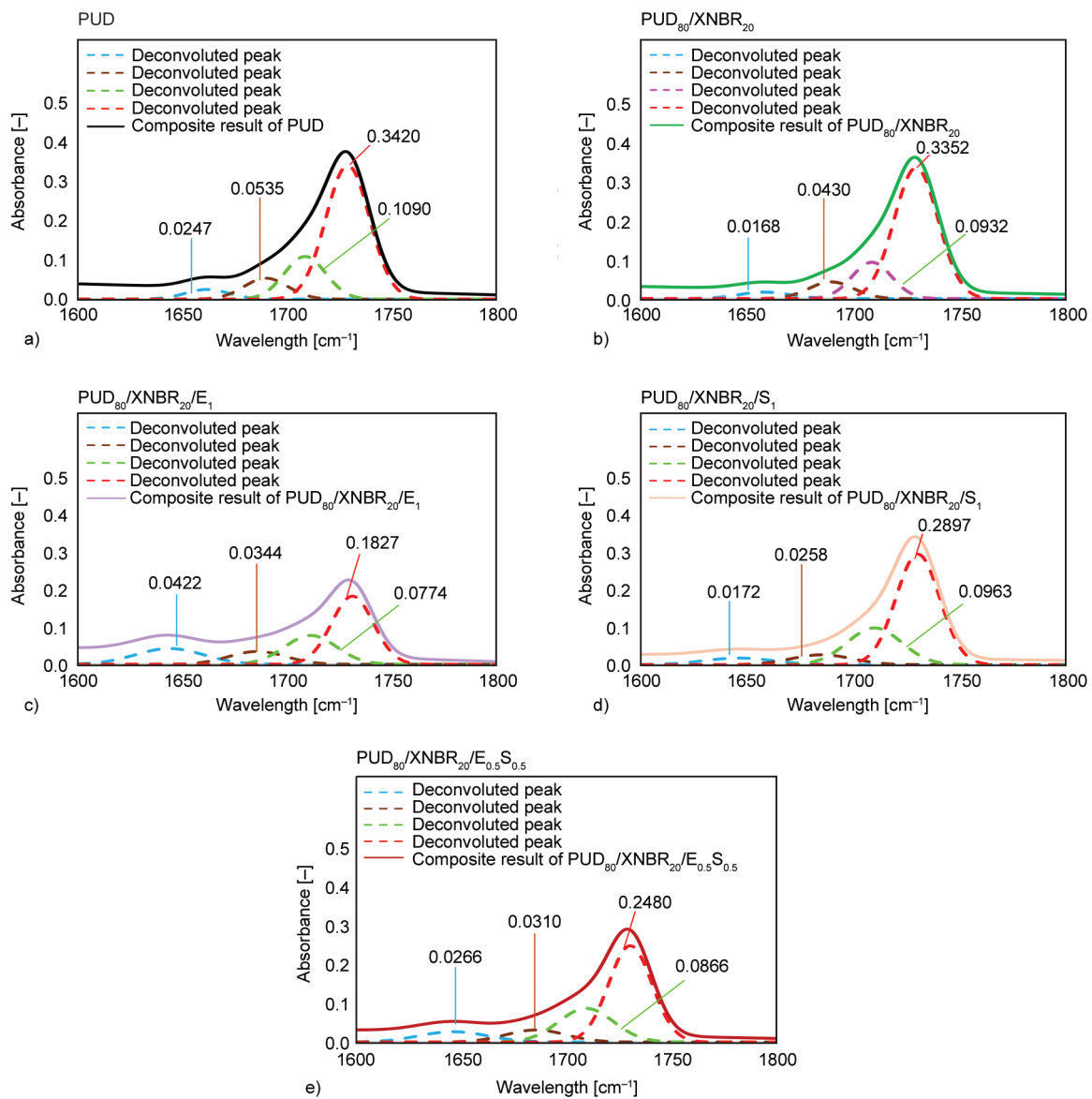


Figure 2. Deconvoluted peak for pristine a) PUD, b) PUD₈₀/XNBR₂₀ blend, and c)–e) PUD₈₀/XNBR₂₀ blends with different types of crosslinkers.

notably in PUD [71, 72]. A total of four peaks were derived and found in the range of 1643–1661, 1685–1689, 1708–1711 and 1728–1731 cm^{-1} [73, 74] as shown in Figure 2. These respective peaks are attributed as follows: hydrogen-bonded polyester in order orientation, order hydrogen-bonded urethane, disordered hydrogen-bonded urethane group, and non-hydrogen-bonded urethane group [37, 75, 76]. The area for each deconvoluted peak, the total degree of hydrogen bonding, and the degree of ordered hydrogen bonding are computed to understand the hydrogen activities within the produced PUD blends. The summary of the respective peaks is listed in Table 3.

Based on the deconvolution results, the degree of hydrogen bonding in the hard segment is reduced after the introduction of XNBR solely in the sample PUD₈₀/XNBR₂₀. As mentioned in the previous discussion, the introduction of the XNBR chain in the PUD interrupted the hydrogen bonding between the hard segments of the PUD and eventually brought the hard segments apart from each other. Apart from that, the degree of hydrogen bonding in the hard segment is found to be increasing when the PUD₈₀/XNBR₂₀ blend is crosslinked with different types of crosslinkers in samples PUD₈₀/XNBR₂₀/E₁, PUD₈₀/XNBR₂₀/S₁ and PUD₈₀/XNBR₂₀/E_{0.5}S_{0.5}, respectively. This also reiterates that the main interaction between PUD, XNBR, and crosslinkers is hydrogen bonding. In addition, it is worth noting that different crosslinkers tend to contribute differently to the hard and soft segments of the PUD.

Furthermore, among the three crosslinked samples, the sample PUD₈₀/XNBR₂₀/S₁ has the highest degree of hydrogen bonding and degree of ordered hydrogen bonding, followed by samples PUD₈₀/XNBR₂₀/E_{0.5}S_{0.5} and PUD₈₀/XNBR₂₀/E₁. This showed that the crosslinker in sample PUD₈₀/XNBR₂₀/E₁ had induced lesser hydrogen bonding activities with PUD compared to the crosslinker in samples

PUD₈₀/XNBR₂₀/S₁ and PUD₈₀/XNBR₂₀/E_{0.5}S_{0.5}. Meanwhile, in the sample PUD₈₀/XNBR₂₀/E_{0.5}S_{0.5}, the combination of the two crosslinkers led to the hydrogen bonding formation positioning between the samples PUD₈₀/XNBR₂₀/E₁ and PUD₈₀/XNBR₂₀/S₁. Besides that, the increment of the degree of hydrogen bonding within the PUD for three of the crosslinked samples also revealed that the incorporation of a crosslinker would encourage the crosslink activities to be carried out among the hard segments of the PUD₈₀/XNBR₂₀ blends, subsequently bringing all the hard segments closer together. This implies that the addition of a crosslinker may improve the strength of the compound, as the hard segment of the PUD is responsible for the mechanical strength of the compound [77].

3.3. Micro- and nano-structure evolution

The determination of micro- and nano-scale surface formation resulting from the interactions of different crosslinkers was examined through AFM. AFM was conducted to observe the micro-surface topography, enabling the evaluation of the surface roughness of the produced PUD₈₀/XNBR₂₀ in the nanometre scale range. The phase image of each respective sample was produced by AFM to understand how the blending system and the crosslinking system would alter the surface structure and surface roughness. Figure 3 shows the topography images and line profiles for pristine PUD, PUD₈₀/XNBR₂₀ blend, and PUD₈₀/XNBR₂₀ blending with different types of crosslinkers. The average surface roughness (S_a), root mean square of roughness (S_q), and maximum height acquired from accordance samples have been tabulated in Table 4. Based on the image in Figure 3, bright and dark regions were unevenly distributed in the sample's topology images. The bright region of the image may represent the hard segment of the PUD, whereas the soft segment is displayed in the dark region in the phase image [62, 78, 79]. This also

Table 3. Area for the respective deconvoluted peak, degree of hydrogen bonding, and degree of ordered hydrogen bonding for the PUD, PUD/XNBR blends and PUD₈₀/XNBR₂₀ blends with different types of crosslinkers.

Materials designation	Area				Degree of hydrogen bonding	Degree of ordered hydrogen bonding
	1643–1661 $[\text{cm}^{-1}]$	1685–1689 $[\text{cm}^{-1}]$	1708–1711 $[\text{cm}^{-1}]$	1728–1730 $[\text{cm}^{-1}]$		
PUD	0.6390	1.3974	2.7005	8.9432	0.346	0.149
PUD ₈₀ /XNBR ₂₀	0.5056	1.1313	2.1853	8.6586	0.306	0.131
PUD ₈₀ /XNBR ₂₀ /E ₁	0.7047	0.9206	3.0763	7.4483	0.387	0.134
PUD ₈₀ /XNBR ₂₀ /S ₁	1.7191	1.1670	2.3936	4.5709	0.591	0.293
PUD ₈₀ /XNBR ₂₀ /E _{0.5} S _{0.5}	1.0823	1.1054	2.8289	6.4003	0.439	0.192

reveals that the surfaces of the produced samples are nonuniform and have different roughness, as the different blending formulations have led to structural diversity and created phase contrast [80]. Based on the data presented in Table 4, it is evident that the values of parameter S_a demonstrate a direct proportional relationship with parameter S_q . The

introduction of XNBR into the formulation of PUD₈₀/XNBR₂₀ led to a reduction in surface roughness for the pristine PUD. Furthermore, the impact of incorporating different types of crosslinkers into PUD₈₀/XNBR₂₀ resulted in varying levels of influence on the surface roughness of the samples, consistent with the corresponding factors, *i.e.*, degree of

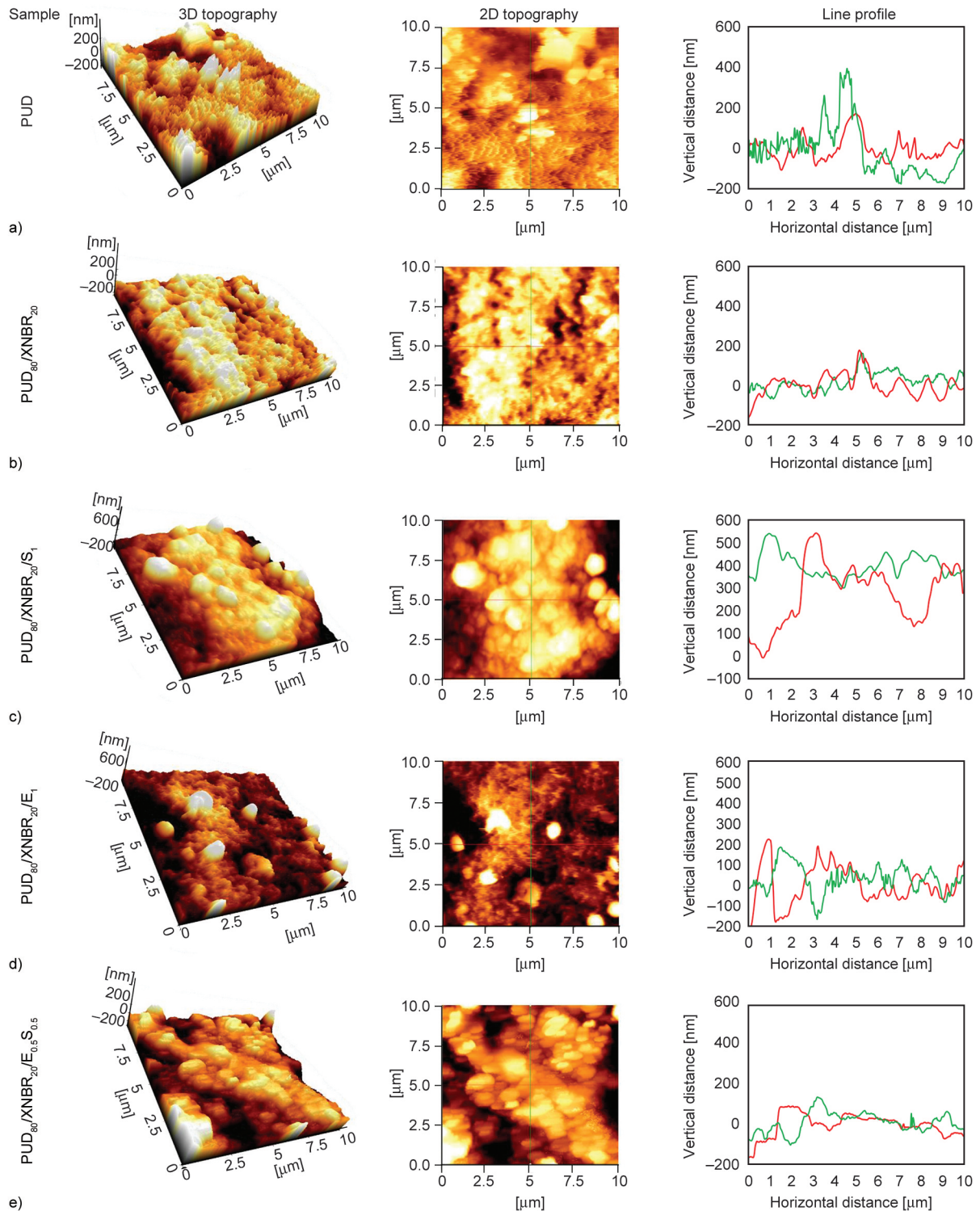


Figure 3. The topography image and line profile for pristine a) PUD, b) PUD₈₀/XNBR₂₀ blend, and c)–e) PUD₈₀/XNBR₂₀ blends with different types of crosslinkers.

Table 4. Roughness analysis for pristine PUD, PUD₈₀/XNBR₂₀ blend, and PUD₈₀/XNBR₂₀ blends with different types of crosslinkers.

Materials designation	S_a [μm]	S_q [μm]	Max. height (red line) [nm]	Max. height (green line) [nm]
PUD	0.064	0.081	171.0	424.8
PUD ₈₀ /XNBR ₂₀	0.048	0.062	148.3	153.5
PUD ₈₀ /XNBR ₂₀ /E ₁	0.081	0.111	199.0	173.0
PUD ₈₀ /XNBR ₂₀ /S ₁	0.275	0.311	539.6	536.9
PUD ₈₀ /XNBR ₂₀ /E _{0.5} S _{0.5}	0.067	0.085	93.1	137.7

ordered hydrogen bonding. To obtain a comprehensive understanding of the correlation between the values of S_a and their association with the degree of ordered hydrogen bonding, graphical representations were employed, illustrating this relationship in Figure 4.

Figure 4 demonstrates a strong correlation between the values of average surface roughness and the degree of ordered hydrogen bonding. In other words, the degree of ordered hydrogen bonding serves as a reliable indicator of the average surface roughness, as higher values of ordered hydrogen bonding correspond to increased average surface roughness values. This also explains that pristine PUD showed a relatively sharp white peak and had a higher maximum height compared to PUD₈₀/XNBR₂₀. This indicated that the incorporation of XNBR into the PUD in the sample PUD₈₀/XNBR₂₀ will create an interruption in the ordered hydrogen bonding of the PUD, causing the height of the hard domain to diminish. This also explained the decrement of the surface roughness S_a and S_q in PUD₈₀/XNBR₂₀, as the ordered hydrogen bonding was distracted by the XNBR chain. This suggested that the order of hydrogen bonding, especially in the hard segment of the PUD, is playing an important role in conferring the surface roughness of the samples, as the disturbance of the hard segment in PUD₈₀/XNBR₂₀ scaled down the surface roughness [81].

Meanwhile, by observation among the crosslinked samples, the sample PUD₈₀/XNBR₂₀/S₁, which introduces an organo-modified siloxane crosslinker, has the highest peak height and the largest size of the bright region compared to other samples. This depicted that the organo-modified siloxane crosslinker had enlarged the hard segment of the PUD by pulling the hard segment closer together through more ordered hydrogen bonding. Similar observations were made by Arévalo-Alquichire *et al.* [80], who observed that the crosslinking system of PU that has more association in the hard segment will tend to have an

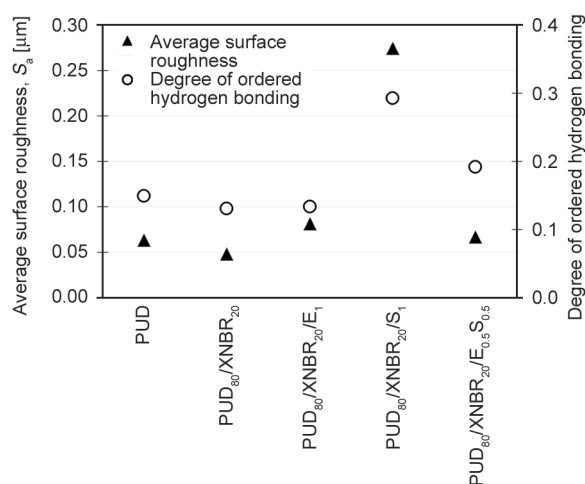


Figure 4. The relationship between the average surface roughness and the degree of ordered hydrogen bonding for pristine PUD, PUD₈₀/XNBR₂₀ blend, and PUD₈₀/XNBR₂₀ blend with different types of crosslinkers.

AFM topology with a great number of big bright regions. In the meantime, the epoxide crosslinker had a lesser bright region and a lower peak height in the sample PUD₈₀/XNBR₂₀/E₁. Besides that, the sample PUD₈₀/XNBR₂₀/E₁ also has a wider dark region compared to the other samples; this also reflects that most of the crosslinking activity may not be dominant in the hard segment, and it is also worth bringing attention to the least degree of hydrogen bonding, particularly in the hard segment, as evidenced by the deconvolution of the FTIR peak in Table 3. The lower height for the brighter region and wider coverage of the soft region of the sample PUD₈₀/XNBR₂₀/E₁ made its surface relatively smoother compared to the sample PUD₈₀/XNBR₂₀/S₁.

For the sample PUD₈₀/XNBR₂₀/E_{0.5}S_{0.5}, which contains both crosslinkers and has quite an even surface with a lesser protrusion of a bright, sharp peak, the height of the bright region is the lowest among the crosslinked samples. This indicated that the combination of these two crosslinkers had created a more uniform hydrogen interaction in both soft and hard

segments, as the line profile of this sample does not have a big fluctuation between the height differences in their surface topology. Unlike the sample PUD₈₀/XNBR₂₀/S1, the line profile showed significant fluctuations as the max height of the topology exceeded 500 nm, but the height of the lower region was in the range of about 10 nm. Owing to the uniform distribution of the surface topology and the lesser fluctuation of the height of the line profile, this further reduced the surface roughness of the sample, making the sample PUD₈₀/XNBR₂₀/E_{0.5}S_{0.5} have the smoothest surface roughness among the crosslinked samples.

In addition, according to the results of FTIR deconvolution, it is evident that the epoxide crosslinkers exhibit the least degree of hydrogen bonding with the hard segment of the PUD. This observation suggests that the epoxide crosslinker primarily interacts with the XNBR, facilitating crosslinking between the XNBR and the C=O groups from the soft segment of the PUD. Conversely, the organo-modified siloxane demonstrates a greater propensity to crosslink between adjacent hard segments of the PUD. This is exemplified by the sample PUD₈₀/XNBR₂₀/S₁, which exhibits the highest degree of hydrogen bonding in the urethane group among all the samples. This difference implies that the epoxide crosslinker is more inclined towards bridging XNBR with the soft segment of the PUD. At the same time, the organo-modified siloxane predominantly connects the hard segments of the PUD with adjacent hard segments. Incorporating these two types of crosslinkers results in a well-connected hard segment of the PUD and an effective linkage between the soft segment of the PUD and XNBR. Consequently, the homogeneity of the blend has improved, as corroborated by AFM studies. In short, the distinct behaviour of epoxide and organo-modified siloxane crosslinkers in facilitating crosslinking interactions between PUD and XNBR underscores their respective roles in enhancing blend homogeneity and performance.

Furthermore, the surface roughness measurements stand out as a significant indicator of the benefits of the hybrid crosslinker. In comparison to the study done by Krzemińska *et al.* [82], the average surface roughness of XNBR film cured with sulphur is approximately 0.239 μm ; on the other hand, this present study showcases markedly reduced surface roughness values for the sulphur-free PUD/XNBR

blends, measuring at 0.048 μm . Notably, blends employing single crosslinkers exhibit higher surface roughness values, reaching 0.081 μm for the epoxide crosslinker and 0.275 μm for the organo-modified siloxane crosslinker. However, by introducing the hybrid crosslinker and its unique hydrogen bonding interactions, the surface roughness can be reduced significantly to 0.067 μm . This emphasises the role of the hybrid crosslinker in fostering a smoother surface for the PUD/XNBR blend. The latex blend with appropriate surface roughness is essential not only to obtain mechanical properties but also for the easy donning process and for the user's comfort during usage.

4. Conclusions

Incorporating a combination of epoxide crosslinkers and siloxane crosslinkers appears to be an effective strategy for producing a PUD/XNBR blend free from sulphur and accelerators. The blending of XNBR and different functional groups of crosslinkers has resulted in multiple types of hydrogen bonding interactions, considerably impacting the total degree of hydrogen bonding and the degree of ordered hydrogen bonding. Notably, the epoxide crosslinker demonstrated a higher propensity for hydrogen bonding interaction within XNBR and PUD, whereas the siloxane crosslinker prefers hydrogen bonding that connects adjacent PUD chains. These various types of hydrogen bonding interactions confer different degrees of ordered hydrogen bonding in the compounds. A higher degree of ordered hydrogen bonding could be associated with a higher surface roughness for the crosslinked PUD/XNBR blends. With the collaboration of both crosslinkers, an advantageous balance of hydrogen between XNBR and PUD is achieved, encouraging the optimal degree of ordered hydrogen bonding and achieving superior performance among all the compounds. The PUD/XNBR blends with hybrid crosslinkers can offer smoother surface roughness, giving rise to easier donning and good colloidal stability that can ensure good quality in the storage and dipping processes of the latex blends. In addition, it is worth mentioning some of the extra benefits offered by the crosslinkers, such as the organo-modified siloxane crosslinkers being able to be used at relatively low temperatures, which can increase energy efficiency during manufacturing. In contrast, the epoxy crosslinkers can enhance the adhesion properties of the latex

blends. Thus, hybrid crosslinkers are feasible for obtaining desirable properties from latex blends for glove applications.

Acknowledgements

The authors would like to express their gratitude to Le Inoova Sdn Bhd for providing external industry funding (304/PBAHAN/6050480/L134).

References

- [1] García-Pacios V., Jofre-Reche J. A., Costa V., Colera M., Martín-Martínez J. M.: Coatings prepared from waterborne polyurethane dispersions obtained with polycarbonates of 1,6-hexanediol of different molecular weights. *Progress in Organic Coatings*, **76**, 1484–1493 (2013).
<https://doi.org/10.1016/j.porgcoat.2013.06.005>
- [2] Patel C. J., Mannari V.: Air-drying bio-based polyurethane dispersion from cardanol: Synthesis and characterization of coatings. *Progress in Organic Coatings*, **77**, 997–1006 (2014).
<https://doi.org/10.1016/j.porgcoat.2014.02.006>
- [3] Sawpan M. A.: Polyurethanes from vegetable oils and applications: A review. *Journal of Polymer Research*, **25**, 184 (2018).
<https://doi.org/10.1007/s10965-018-1578-3>
- [4] Das A., Mahanwar P.: A brief discussion on advances in polyurethane applications. *Advanced Industrial and Engineering Polymer Research*, **3**, 93–101 (2020).
<https://doi.org/10.1016/j.aiepr.2020.07.002>
- [5] Song S. C., Choi H. H., Park K.-K., Park Y. G., Lee S., Im D., Lee W. K.: Synthesis and properties of waterborne polyurethane dispersions for surface coatings on poly(vinyl chloride). *Molecular Crystals and Liquid Crystals*, **706**, 101–107 (2020).
<https://doi.org/10.1080/15421406.2020.1743444>
- [6] Roland C. D., Moore C. M., Leal J. H., Semelsberger T. A., Snyder C., Kostal J., Sutton A. D.: Fully recyclable polycarbonates from simple, bio-derived building blocks. *ACS Applied Polymer Materials*, **3**, 730–736 (2021).
<https://doi.org/10.1021/acsapm.0c01028>
- [7] Avar G., Meier-Westhues U., Casselmann H., Achten D.: Polyurethanes. in ‘Polymer science: A comprehensive reference’ (eds.: Möller M., Matyjaszewski K.) Elsevier, Amsterdam, 411–441 (2012).
<https://doi.org/10.1016/B978-0-444-53349-4.00275-2>
- [8] Peng H., Du X., Cheng X., Wang H., Du Z.: Room-temperature self-healable and stretchable waterborne polyurethane film fabricated via multiple hydrogen bonds. *Progress in Organic Coatings*, **151**, 106081 (2021).
<https://doi.org/10.1016/j.porgcoat.2020.106081>
- [9] Tas C. E., Berksun E., Koken D., Unal S., Unal H.: Photothermal waterborne polydopamine/polyurethanes with light-to-heat conversion properties. *ACS Applied Polymer Materials*, **3**, 3929–3940 (2021).
<https://doi.org/10.1021/acsapm.1c00495>
- [10] Noreen A., Zia K. M., Zuber M., Tabasum S., Zahoor A. F.: Bio-based polyurethane: An efficient and environment friendly coating systems: A review. *Progress in Organic Coatings*, **91**, 25–32 (2016).
<https://doi.org/10.1016/j.porgcoat.2015.11.018>
- [11] Liu X., Hong W., Chen X.: Continuous production of water-borne polyurethanes: A review. *Polymers*, **12**, 2875 (2020).
<https://doi.org/10.3390/polym12122875>
- [12] Patel R., Kapatel P.: Waterborne polyurethanes: A three step synthetic approach towards environmental friendly flame retardant coatings. *Progress in Organic Coatings*, **125**, 186–194 (2018).
<https://doi.org/10.1016/j.porgcoat.2018.09.010>
- [13] Man L., Feng Y., Hu Y., Yuan T., Yang Z.: A renewable and multifunctional eco-friendly coating from novel tung oil-based cationic waterborne polyurethane dispersions. *Journal of Cleaner Production*, **241**, 118341 (2019).
<https://doi.org/10.1016/j.jclepro.2019.118341>
- [14] Rashmi E. V., Vijayalakshmi K. P., Balachandran N., Mathew D., Santhosh Kumar K. S.: Soft-segment free polyurethanes and their self-healable films. *Progress in Organic Coatings*, **146**, 105709 (2020).
<https://doi.org/10.1016/j.porgcoat.2020.105709>
- [15] Madbouly S. A.: Waterborne polyurethane dispersions and thin films: Biodegradation and antimicrobial behaviors. *Molecules*, **26**, 961 (2021).
<https://doi.org/10.3390/molecules26040961>
- [16] Behera P. K., Raut S. K., Mondal P., Sarkar S., Singha N. K.: Self-healable polyurethane elastomer based on dual dynamic covalent chemistry using Diels-Alder “click” and disulfide metathesis reactions. *ACS Applied Polymer Materials*, **3**, 847–856 (2021).
<https://doi.org/10.1021/acsapm.0c01179>
- [17] Fan W., Wang J., Li Z.: Antiglare waterborne polyurethane/modified silica nanocomposite with balanced comprehensive properties. *Polymer Testing*, **99**, 107072 (2021).
<https://doi.org/10.1016/j.polymertesting.2021.107072>
- [18] Qian Y., Dong F., Guo L., Xu X., Liu H.: Two-component waterborne polyurethane modified with terpene derivative-based polysiloxane for coatings via a thiolene click reaction. *Industrial Crops and Products*, **171**, 113903 (2021).
<https://doi.org/10.1016/j.indcrop.2021.113903>
- [19] Li F., Liang Z., Li Y., Wu Z., Yi Z.: Synthesis of waterborne polyurethane by inserting polydimethylsiloxane and constructing dual crosslinking for obtaining the superior performance of waterborne coatings. *Composites Part B: Engineering*, **238**, 109889 (2022).
<https://doi.org/10.1016/j.compositesb.2022.109889>

- [20] Pandya H., Mahanwar P.: Fundamental insight into anionic aqueous polyurethane dispersions. *Advanced Industrial and Engineering Polymer Research*, **3**, 102–110 (2020).
<https://doi.org/10.1016/j.aiepr.2020.07.003>
- [21] Fang Z. H., Duan H. Y., Zhang Z. H., Wang J., Li D. Q., Huang Y. X., Shang J. J., Liu Z. Y.: Novel heat-resistance UV curable waterborne polyurethane coatings modified by melamine. *Applied Surface Science*, **257**, 4765–4768 (2011).
<https://doi.org/10.1016/j.apsusc.2010.10.082>
- [22] Ismoilov K., Akram W., Chauhan S., Ergasheva K., Artikboeva R., Islomova Z., Quan H.: Synthesis and evaluation of properties of a novel cationic waterborne polyurethane finishing agent. *Journal of Chemical Engineering and Process Technology*, **10**, 398 (2019).
<https://doi.org/10.35248/2157-7048.19.10.398>
- [23] Tahir M., Heinrich G., Mahmood N., Boldt R., Wießner S., Stöckelhuber K. W.: Blending *in situ* polyurethane-urea with different kinds of rubber: Performance and compatibility aspects. *Materials*, **11**, 2175 (2018).
<https://doi.org/10.3390/ma11112175>
- [24] Yan H., Li H., Li W., Fan X., Zhang L., Zhu M.: Probing the damping property of three-dimensional graphene aerogels in carboxylated nitrile butadiene rubber/polyurethane blend. *Polymer Engineering and Science*, **60**, 61–70 (2019).
<https://doi.org/10.1002/pen.25259>
- [25] Yew G. Y., Tham T. C., Law C. L., Chu D-T., Ogino C., Show P. L.: Emerging crosslinking techniques for glove manufacturers with improved nitrile glove properties and reduced allergic risks. *Materials Today Communications*, **19**, 39–50 (2018).
<https://doi.org/10.1016/j.mtcomm.2018.12.014>
- [26] Ai C., Gong G., Zhao X., Liu P.: Determination of carboxyl content in carboxylated nitrile butadiene rubber (XNBR) after degradation *via* olefin cross metathesis. *Polymer Testing*, **60**, 250–252 (2017).
<https://doi.org/10.1016/j.polymertesting.2017.04.004>
- [27] Lipińska M., Gaca M., Zaborski M.: Curing kinetics and ionic interactions in layered double hydroxides–nitrile rubber Mg–Al-LDHs–XNBR composites. *Polymer Bulletin*, **78**, 3199–3226 (2021).
<https://doi.org/10.1007/s00289-020-03249-6>
- [28] Düşünceli N., Akyüz L., Şahin N., Duru H.: The effect of polyurethane and carnauba wax on the mechanical and physicochemical properties of acrylonitrile butadiene nitrile rubber coating working gloves. *Journal of Elastomers and Plastics*, **51**, 36–51 (2018).
<https://doi.org/10.1177/0095244318768650>
- [29] Ning N., Qin H., Wang M., Sun H., Tian M., Zhang L.: Improved dielectric and actuated performance of thermoplastic polyurethane by blending with XNBR as macromolecular dielectrics. *Polymer*, **179**, 121646 (2019).
<https://doi.org/10.1016/j.polymer.2019.121646>
- [30] Kohári A., Halász I. Z., Bárányi T.: Thermoplastic dynamic vulcanizates with *in situ* synthesized segmented polyurethane matrix. *Polymers*, **11**, 1663 (2019).
<https://doi.org/10.3390/polym11101663>
- [31] Zhang G., Feng H., Liang K., Wang Z., Li X., Zhou X., Guo B., Zhang L.: Design of next-generation cross-linking structure for elastomers toward green process and a real recycling loop. *Science Bulletin*, **65**, 889–898 (2020).
<https://doi.org/10.1016/j.scib.2020.03.008>
- [32] Magg H.: Crosslinking of carboxylated nitrile rubbers with resol resins. *International Polymer Science and Technology*, **40**, 1–10 (2013).
<https://doi.org/10.1177/0307174x1304000901>
- [33] Lenko D., Schlögl S., Temel A., Schaller R., Holzner A., Kern W.: Dual crosslinking of carboxylated nitrile butadiene rubber latex employing the thiol-ene photoreaction. *Journal of Applied Polymer Science*, **129**, 2735–2743 (2013).
<https://doi.org/10.1002/app.38983>
- [34] Laskowska A., Zaborski M., Boiteux G., Gain O., Marzec A., Maniukiewicz W.: Ionic elastomers based on carboxylated nitrile rubber (XNBR) and magnesium aluminum layered double hydroxide (hydrotalcite). *Express Polymer Letters*, **8**, 374–386 (2014).
<https://doi.org/10.3144/expresspolymlett.2014.42>
- [35] Laskowska A., Zaborski M., Boiteux G., Gain O., Marzec A., Maniukiewicz W.: Effects of unmodified layered double hydroxides MgAl-LDHs with various structures on the properties of filled carboxylated acrylonitrile-butadiene rubber XNBR. *European Polymer Journal*, **60**, 172–185 (2014).
<https://doi.org/10.1016/j.eurpolymj.2014.09.013>
- [36] Yang S., Fan H., Jiao Y., Cai Z., Zhang P., Li Y.: Improvement in mechanical properties of NBR/LiClO₄/POSS nanocomposites by constructing a novel network structure. *Composites Science and Technology*, **138**, 161–168 (2017).
<https://doi.org/10.1016/j.compscitech.2016.12.003>
- [37] Balaban M., Antić V., Pergal M., Francolini I., Martinelli A., Djonlagić J.: The effect of the polar solvents on the synthesis of poly(urethane-urea-siloxane)s. *Journal of the Serbian Chemical Society*, **77**, 1457–1481 (2012).
<https://doi.org/10.2298/JSC111025056B>
- [38] Liu Y., Meng Z., Wang Y., Li P., Sun Y.: Analysis and modeling of viscosity for aqueous polyurethane dispersion as a function of shear rate, temperature, and solid content. *ACS Omega*, **5**, 26237–26244 (2020).
<https://doi.org/10.1021/acsomega.0c03959>
- [39] Liang H., Wang S., He H., Wang M., Liu L., Lu J., Zhang Y., Zhang C.: Aqueous anionic polyurethane dispersions from castor oil. *Industrial Crops and Products*, **122**, 182–189 (2018).
<https://doi.org/10.1016/j.indcrop.2018.05.079>

- [40] Ye G., Jiang T.: Preparation and properties of self-healing waterborne polyurethane based on dynamic disulfide bond. *Polymers*, **13**, 2936 (2021).
<https://doi.org/10.3390/polym13172936>
- [41] Sis H., Birinci M.: Effect of nonionic and ionic surfactants on zeta potential and dispersion properties of carbon black powders. *Colloids and Surfaces A: Physicochemical and Engineering Aspects*, **341**, 60–67 (2009).
<https://doi.org/10.1016/j.colsurfa.2009.03.039>
- [42] Oh J. K., Yegin Y., Yang F., Zhang M., Li J., Huang S., Verkhoturov S. V., Schweikert E. A., Perez-Lewis K., Scholar E. A., Taylor T. M., Castillo A., Cisneros-Zevallos L., Min Y., Akbulut M.: The influence of surface chemistry on the kinetics and thermodynamics of bacterial adhesion. *Scientific Reports*, **8**, 17247 (2018).
<https://doi.org/10.1038/s41598-018-35343-1>
- [43] Rahman M. M.: Stability and properties of waterborne polyurethane/clay nanocomposite dispersions. *Journal of Coatings Technology and Research*, **14**, 1357–1368 (2017).
<https://doi.org/10.1007/s11998-017-9944-3>
- [44] Nuraini L., Triwulandari E., Ghozali M., Hanafi M., Jumina J.: Synthesis of polyurethane/silica modified epoxy polymer based on 1,3-propanediol for coating application. *Indonesian Journal of Chemistry*, **17**, 477–484 (2017).
<https://doi.org/10.22146/ijc.22321>
- [45] Phung H., Schacht E., du Prez F., Gelan J., Adriaesens P., Storme L.: Crosslinked polyurethane-based gels. *Polymer Journal*, **35**, 353–358 (2003).
<https://doi.org/10.1295/polymj.35.353>
- [46] Apekis L., Pissis P., Christodoulides C., Spathis G., Niaounakis M., Kontou E., Schlosser E., Schönhals A., Goering H.: Physical and chemical network effects in polyurethane elastomers. *Colloid and Polymer Science*, **268**, 636–644 (1990).
<https://doi.org/10.1007/bfb0115492>
- [47] Kapatel P., Patel R.: Flame retardant waterborne polyurethanes: Synthesis, characterization, and evaluation of different properties. *Biointerface Research in Applied Chemistry*, **12**, 3198–3214 (2022).
<https://doi.org/10.33263/BRIAC123.31983214>
- [48] Ding J. N., Fan Y., Zhao C. X., Liu Y. B., Yu C. T., Yuan N. Y.: Electrical conductivity of waterborne polyurethane/graphene composites prepared by solution mixing. *Journal of Composite Materials*, **46**, 747–752 (2012).
<https://doi.org/10.1177/0021998311413835>
- [49] Chen S., Wang T., Wang Q., Pei X.: Damping properties of polyurethane/epoxy graft interpenetrating polymer network composites filled with short carbon fiber and nano-SiO₂. *Journal of Macromolecular Science Part B: Physics*, **50**, 931–941 (2011).
<https://doi.org/10.1080/00222348.2010.497068>
- [50] Hao H., Hu J. Q., Tu W. P.: Preparation and properties of high storage stability polyester polyol dispersion for two-component waterborne polyurethane coating. *Journal of Physics: Conference Series*, **755**, 012067 (2016).
<https://doi.org/10.1088/1757-899X/167/1/012067>
- [51] Delpech M. C., Miranda G. S.: Waterborne polyurethanes: Influence of chain extender in FTIR spectra profiles. *Central European Journal of Engineering*, **2**, 231–238 (2012).
<https://doi.org/10.2478/s13531-011-0060-3>
- [52] Dai M., Wang J., Zhang Y.: Improving water resistance of waterborne polyurethane coating with high transparency and good mechanical properties. *Colloids and Surfaces A: Physicochemical and Engineering Aspects*, **601**, 124994 (2020).
<https://doi.org/10.1016/j.colsurfa.2020.124994>
- [53] Samantarai S., Nag A., Singh N., Dash D., Basak A., Nando G. B., Das N. C.: Chemical modification of nitrile rubber in the latex stage by functionalizing phosphorylated cardanol prepolymer: A bio-based plasticizer and a renewable resource. *Journal of Elastomers and Plastics*, **51**, 99–129 (2019).
<https://doi.org/10.1177/0095244318768644>
- [54] Sadeghalvaad M., Dabiri E., Zahmatkesh S., Afsharimoghdam P.: Preparation and properties evaluation of nitrile rubber nanocomposites reinforced with organo-clay, CaCO₃, and SiO₂ nanofillers. *Polymer Bulletin*, **76**, 3819–3839 (2018).
<https://doi.org/10.1007/s00289-018-2583-8>
- [55] Kapgate B. P., Das C., Basu D., Das A., Heinrich G.: Rubber composites based on silane-treated stöber silica and nitrile rubber: Interaction of treated silica with rubber matrix. *Journal of Elastomers and Plastics*, **47**, 248–261 (2015).
<https://doi.org/10.1177/0095244313507807>
- [56] Zhang Y., Zhao M., Zhang J., Shao Q., Li J., Li H., Lin B., Yu M., Chen S., Guo Z.: Excellent corrosion protection performance of epoxy composite coatings filled with silane functionalized silicon nitride. *Journal of Polymer Research*, **25**, 130 (2018).
<https://doi.org/10.1007/s10965-018-1518-2>
- [57] Zia K. M., Ahmad A., Anjum S., Zuber M., Anjum M. N.: Synthesis and characterization of siloxane-based polyurethane elastomers using hexamethylene diisocyanate. *Journal of Elastomers and Plastics*, **47**, 625–635 (2015).
<https://doi.org/10.1177/0095244314526746>
- [58] Su X., Yu Y., Li B., Wang J., Lu C., Zong J., Li J., Wang F.: Synthesis and characterization of polyurethane-poly-siloxane block copolymers modified by α,ω -hydroxyalkyl polysiloxanes with methacrylate side chain. *Science and Engineering of Composite Materials*, **28**, 528–539 (2021).
<https://doi.org/10.1515/secm-2021-0052>

- [59] Sousa R. P. C. L., Figueira R. B., Gomes B. R., Sousa S., Ferreira R. C. M., Costa S. P. G., Raposo M. M. M.: Hybrid sol-gel matrices doped with colorimetric/fluorimetric imidazole derivatives. *Nanomaterials*, **11**, 3401 (2021).
<https://doi.org/10.3390/nano11123401>
- [60] Pierpoint S., Silverman J., Al-Sheikhly M.: Effects of ionizing radiation on the aging of polyester based polyurethane binder. *Radiation Physics and Chemistry*, **62**, 163–169 (2001).
[https://doi.org/10.1016/S0969-806X\(01\)00434-0](https://doi.org/10.1016/S0969-806X(01)00434-0)
- [61] Bahadur A., Shoaib M., Saeed A., Iqbal S.: FT-IR spectroscopic and thermal study of waterborne polyurethane-acrylate leather coatings using tartaric acid as an ionomer. *E-Polymers*, **16**, 463–474 (2016).
<https://doi.org/10.1515/epoly-2016-0154>
- [62] Oprea S., Potolinca V-O., Oprea V.: Synthesis and properties of new crosslinked polyurethane elastomers based on isosorbide. *European Polymer Journal*, **83**, 161–172 (2016).
<https://doi.org/10.1016/j.eurpolymj.2016.08.020>
- [63] Ma S., Liu W., Wei Z., Li H.: Mechanical and thermal properties and morphology of epoxy resins modified by a silicon compound. *Journal of Macromolecular Science Part A: Pure and Applied Chemistry*, **47**, 1084–1090 (2010).
<https://doi.org/10.1080/10601325.2010.511522>
- [64] Byczyński Ł.: Effect of different polyethers on surface and thermal properties of poly(urethane-siloxane) copolymers modified with side-chain siloxane. *Journal of Thermal Analysis and Calorimetry*, **114**, 397–408 (2013).
<https://doi.org/10.1007/s10973-012-2903-4>
- [65] Schmidt P., Dybal J., Šturcová A.: ATR FTIR investigation of interactions and temperature transitions of poly(ethylene oxide), poly(propylene oxide) and ethylene oxide–propylene oxide–ethylene oxide tri-block copolymers in water media. *Vibrational Spectroscopy*, **50**, 218–225 (2009).
<https://doi.org/10.1016/j.vibspec.2008.12.003>
- [66] Dai Z., Yang K., Dong Q.: Synthesis and characterization of hydroxy-terminated polyether-polydimethylsiloxane-polyether (PE-PDMS-PE) triblock oligomers and their use in the preparation of thermoplastic polyurethanes. *Journal of Applied Polymer Science*, **132**, 42521 (2015).
<https://doi.org/10.1002/app.42521>
- [67] Zeng D., Liu Z., Bai S., Zhao J., Wang J.: Corrosion resistance of bis-silane-modified epoxy coatings on an Al-Zn-Mg-Cu alloy. *Journal of Materials Engineering and Performance*, **29**, 5282–5290 (2020).
<https://doi.org/10.1007/s11665-020-05049-5>
- [68] Caldara M., Colleoni C., Guido E., Re V., Rosace G.: Optical monitoring of sweat pH by a textile fabric wearable sensor based on covalently bonded litmus-3-glycidoxypropyltrimethoxysilane coating. *Sensors and Actuators, B: Chemical*, **222**, 213–220 (2016).
<https://doi.org/10.1016/j.snb.2015.08.073>
- [69] Tanaka T., Yokoyama T., Yamaguchi Y.: Quantitative study on hydrogen bonding between urethane compound and ethers by infrared spectroscopy. *Journal of Polymer Science*, **6**, 2137–2152 (1968).
<https://doi.org/10.1002/pol.1968.150060811>
- [70] Mattia J., Painter P.: A comparison of hydrogen bonding and order in a polyurethane and poly(urethane-urea) and their blends with poly(ethylene glycol). *Macromolecules*, **40**, 1546–1554 (2007).
<https://doi.org/10.1021/ma0626362>
- [71] Costa V., Nohales A., Félix P., Guillem C., Gómez C. M.: Enhanced polyurethanes based on different polycarbonatediols. *Journal of Elastomers and Plastics*, **45**, 217–238 (2013).
<https://doi.org/10.1177/0095244312452274>
- [72] Yang S., Wang S., Du X., Du Z., Cheng X., Wang H.: Mechanically robust self-healing and recyclable flame-retarded polyurethane elastomer based on thermoreversible crosslinking network and multiple hydrogen bonds. *Chemical Engineering Journal*, **391**, 123544 (2020).
<https://doi.org/10.1016/j.cej.2019.123544>
- [73] Špírková M., Pavličević J., Strachota A., Poreba R., Bera O., Kaprálková L., Baldrian J., Šlouf M., Lazić N., Budinski-Simendić J.: Novel polycarbonate-based polyurethane elastomers: Composition-property relationship. *European Polymer Journal*, **47**, 959–972 (2011).
<https://doi.org/10.1016/j.eurpolymj.2011.01.001>
- [74] Król B., Król P., Byczyński Ł., Szałański P.: Methods of increasing hydrophobicity of polyurethane materials: Important applications of coatings with low surface free energy. *Colloid and Polymer Science*, **295**, 2309–2321 (2017).
<https://doi.org/10.1007/s00396-017-4202-x>
- [75] Güney A., Kiziltay A., Hasirci N., Tanir T. E.: Synthesis and characterization of polycaprolactone-based segmented polyurethanes. *Turkish Journal of Chemistry*, **43**, 452–463 (2019).
<https://doi.org/10.3906/kim-1801-44>
- [76] Głowińska E., Kasprzyk P., Datta J.: The green approach to the synthesis of bio-based thermoplastic polyurethane elastomers with partially bio-based hard blocks. *Materials*, **14**, 2334 (2021).
<https://doi.org/10.3390/ma14092334>
- [77] Korley L. S. T. J., Pate B. D., Thomas E. L., Hammond P. T.: Effect of the degree of soft and hard segment ordering on the morphology and mechanical behavior of semicrystalline segmented polyurethanes. *Polymer*, **47**, 3073–3082 (2006).
<https://doi.org/10.1016/j.polymer.2006.02.093>
- [78] Fan X., Lv Z., Zu X.: Study on microphase separation of novel crosslinked polyurethane by AFM and DMA. *Revue Roumaine de Chimie*, **64**, 225–231 (2019).
<https://doi.org/10.33224/rch/2019.64.3.03>

- [79] Cheng B-X., Gao W-C., Ren X-M., Ouyang X-Y., Zhao Y., Zhao H., Wu W., Huang C-X., Liu Y., Liu X-Y., Li H-N., Li R. K. Y.: A review of microphase separation of polyurethane: Characterization and applications. *Polymer Testing*, **107**, 107489 (2022).
<https://doi.org/10.1016/j.polymertesting.2022.107489>
- [80] Arévalo-Alquichire S., Morales-Gonzalez M., Navas-Gómez K., Diaz L. E., Gómez-Tejedor J. A., Serrano M. A., Valero M. F.: Influence of polyol/crosslinker blend composition on phase separation and thermo-mechanical properties of polyurethane thin films. *Polymers*, **12**, 666 (2020).
<https://doi.org/10.3390/polym12030666>
- [81] Oprea S., Oprea V.: Synthesis and characterization of the cross-linked polyurethane-gum arabic blends obtained by multiacrylates cross-linking polymerization. *Journal of Elastomers and Plastics*, **45**, 564–576 (2013).
<https://doi.org/10.1177/0095244312459281>
- [82] Krzemińska S. M., Smejda-Krzewicka A. A., Leniart A., Lipińska L., Woluntarski M.: Effects of curing agents and modified graphene oxide on the properties of XNBR composites. *Polymer Testing*, **83**, 106368 (2020).
<https://doi.org/10.1016/j.polymertesting.2020.106368>